Applied Physics Letters

Enhanced bulk photovoltaic response in Sn doped $BaTiO_3$ through composition dependent structural transformation

Cite as: Appl. Phys. Lett. **114**, 183901 (2019); https://doi.org/10.1063/1.5088635
Submitted: 12 January 2019 . Accepted: 24 April 2019 . Published Online: 07 May 2019

Lakshmi Kola, D. Murali, Subhajit Pal, B. R. K. Nanda, and P. Murugavel

Applied Physics Letters ARTICLE scitation.org/journal/apl

Enhanced bulk photovoltaic response in Sn doped $BaTiO_3$ through composition dependent structural transformation

Cite as: Appl. Phys. Lett. **114**, 183901 (2019); doi: 10.1063/1.5088635
Submitted: 12 January 2019 · Accepted: 24 April 2019 ·
Published Online: 7 May 2019

Lakshmi Kola, D. Murali, Subhajit Pal, B. R. K. Nanda, and P. Murugavel[a)]

AFFILIATIONS

Department of Physics, Indian Institute Technology Madras, Chennai 600036, India

[a)]Author to whom correspondence should be addressed: muruga@iitm.ac.in

ABSTRACT

Polycrystalline $BaTi_{1-x}Sn_xO_3$ samples ($x = 0.06$, 0.07, 0.08, 0.09, 0.10, and 0.11) were synthesized by the solid state technique. The samples exhibit the tetragonal phase at 300 K. In addition, the samples $x = 0.06$, 0.07, 0.08, and 0.09 also show the orthorhombic phase with enhanced phase fractions upon poling. However, the % orthorhombic phase fractions show an increase up to $x = 0.07$ and a decrease with an increase in x. The dielectric studies indicate that T_C (cubic to tetragonal phase transition) shifts toward lower temperature where the samples $x = 0.10$ and 0.11 show the tetragonal phase at 300 K. The samples exhibit the maximum remnant polarization and piezoelectric coefficient for $x = 0.08$. But the bandgap for the $x = 0.07$ sample shows the value of 2.61 eV before poling and 2.95 eV after poling. A giant photovoltaic (PV) response is seen in the samples with the open-circuit voltage (V_{OC}) as large as 16 V (for $x = 0.07$). V_{OC} shows a decreasing trend with an increase in the Sn content after $x = 0.07$, and it did not follow the trend in polarization and the bandgap. The observed results are correlated with the structural symmetry of the compound, and they are validated by the band-structure calculations. The experimental and theoretical studies indicate that the sample with the orthorhombic phase is preferable for the enhanced photovoltaic response in comparison to the tetragonal phase. These studies show a new way to achieve a large photovoltaic response so as to design the system for several device applications such as UV detectors and microactuators.

During the last few decades, the development of semiconductor photovoltaic (PV) cells has cause them to emerge as a significant clean energy resource. However, V_{OC} being lower than the bandgap of the semiconductors becomes a hindrance for their further advancement. In recent times, various new materials have been studied for enhanced PV properties.[1–5] Among them, ferroelectric systems have gained huge interest due to their observed above bandgap photovoltage in bulk.[6–9] Note that the PV effect in ferroelectrics is known since the 1970s when a large PV response was reported on single crystals of Fe doped $LiNbO_3$.[10] Off late, several factors such as electric polarization, crystal symmetry, electrode spacing, and ferroelectric/electrode interface are reported to affect the PV response in ferroelectric bulk and thin film geometries.[11–15] Accordingly, various theories have been formulated in order to explain the unconventional PV response in ferroelectrics.[16]

Earlier, the mechanism of electron-hole pair separation in a ferroelectric material is perceived to arise from the internal electric field originated from the polarization. Recently, the domain wall theory has been proposed to explain the large PV response observed in the $BiFeO_3$ thin film, where the illuminated domain walls act as nanoscale photovoltage generators connected in series.[17] However, it is generally accepted that the Schottky junctions and depolarization fields influence V_{OC} in ferroelectric films.[16] Neverthless, the major contributions to the PV effect in bulk ferroelectric samples are explained by the ballistic and shift current models.[8,18–21] According to the ballistic mechanism, the generation of photocurrent in non-centrosymmetric ferroelectric crystals is correlated with the asymmetric momentum distributions of photo-generated charge carriers in the conduction band.[10] On the other hand, the shift current mechanism is associated with the inter-band transition of photo-generated charge carriers with a virtual shift of the momentum vector in real space in non-centrosymmetric systems and hence results in a large PV effect.[18–21] In this context, the recent report on $KNbO_3$ and $(K,Ba)(Ni,Nb)O_{3-\delta}$ systems elucidated a strong correlation between the electronic structure and the PV response.[22] Importantly, their calculations showed the structural preference for shift current, where the ferroelectric system having rhombohedral and orthorhombic (O) symmetry revealed a

large shift current coefficient than the system having tetragonal (T) symmetry. Interestingly, the reported large PV response in $Pb_{1-x}La_x(Zr_yTi_{1-y})_{1-x/4}O_3$ having the coexistence of multiple phases strongly suggests the structural preference for the effective PV response.[23]

In this regard, the recently studied lead free ferroelectric $BaTi_{1-x}Sn_xO_3$ (BST) system showing superior ferroelectric and piezoelectric characteristics attracts large research interest.[24] Importantly, BST is reported to exhibit various structural transitions whose transition temperatures can be tuned by Sn doping.[24] These characteristics enable the BST sample to be one of the potential candidates to show a large PV effect and to understand its structural correlations. However, the PV studies are unexplored in this highly significant compound. In the present work, PV characteristics are investigated on selected compositions ($x = 0.06$, 0.07, 0.08, 0.09, 0.10, and 0.11) of polycrystalline BST samples. These compositions are selected based on their reported high piezoelectric coefficient (d_{33}) values.[25] Notably, the samples revealed a giant composition dependent PV response with the maximum V_{OC} value of 16 V for the $x = 0.07$ sample. The observed results are correlated with the structural symmetry of the compound, and they are validated by the band-structure calculations.

BST samples with compositions of $x = 0.06$, 0.07, 0.08, 0.09, 0.10, and 0.11 were fabricated by the solid state method. Stoichiometric amounts of the precursors $BaCO_3$, TiO_2, and SnO_2 were ground in an agate mortar and calcined at 1200 °C for 4 h. The uniaxially pressed pellets made from the calcined powders were sintered at 1400 °C for 4 h. The compositions $x = 0.06$, 0.07, 0.08, 0.09, 0.10, and 0.11 are selected on account of their high d_{33} values, where the composition $x = 0.08$ shows the highest (296 pC/N) value.[25] The samples $x = 0.06$, 0.07, 0.08, 0.09, 0.10, and 0.11 are referred to as BST6, BST7, BST8, BST9, BST10, and BST11, respectively. Note that these compositions are nominal compositions estimated from the weighted fractions of the precursors added during the synthesis. The X-ray diffraction (XRD) using a Rigaku SmartLab X-ray diffractometer is performed for phase verification. The structural parameters are extracted by Rietveld refinement using FULLPROF software. The 8 mm diameter pellets coated with Ag electrodes are used for electrical measurements. A Radiant Technology polarization loop tracer is used for the polarization measurements. The bandgaps of the samples are inferred from the reflectance spectrum obtained using a UV-Visible–Near Infrared Spectrophotometer. For PV measurements, Ag electrodes in a finger geometry (finger thickness 100 μm and gap 200 μm) are thermally coated on the polished surface of pellets (8 mm diameter and 1 mm thickness). The bottom surface coated with Ag paint is used as the bottom electrode. Prior to PV measurements, the samples are poled at a 2.5 kV/mm electric field for 1 h and then shorted overnight to remove parasitic surface charges. PV measurements are carried out using a Xenon-arc lamp (Newport, Model No-67005) as a light source and a Keithley electrometer (6517B) as a measuring unit.

The pseudopotential (PP) based Vienna *ab-initio* Simulation Package (VASP) is used to perform the density functional theory (DFT) calculations.[26] PPs are based on the projected augmented wave (PAW) method[27] with exchange and correlation effects described using the Generalized Gradient Approximation (GGA) and Perdew-Burke-Ernzerhof (PBE) functional.[28,29] For calculations, the valence electrons considered for various elements are Ba-$4s^2$ $4p^6$ $5s^2$, Sn-$4d^{10}5s^25p^2$, Ti-$3p^6$ $3d^2$ $4s^2$, and O-$2s^2$ $2p^4$. The plane wave cut-off energy is chosen as 500 eV. Calculations are performed on T and O phases of $BaTiO_3$. To simulate experimental doping concentrations, we adopted the supercell approach with periodic boundary conditions and performed our calculations using $2 \times 2 \times 3$ and $3 \times 2 \times 1$ supercells corresponding to ferroelectric T (*P4 mm*) and O (*Amm2*) phases, respectively. In each of these supercells, a single Ti ion is replaced by a single Sn ion. For structural optimization, we chose a convergence criterion of 10^{-6} eV for self-consistent field (SCF) electronic energy and 10^{-3} eV/A for Hellmann–Feynman forces on each atom. An $(8 \times 8 \times 8)$ and $(6 \times 8 \times 8)$ Monkhorst–Pack grid[30] is used for the Brillouin Zone integration of bulk T and O BST, respectively. Proportionate *k*-grids are used for the super cells.

The XRD patterns of BST6, BST7, BST8, BST9, BST10, and BST11 samples under un-poled conditions are recorded at 300 K, and they are fitted with Rietveld refinement using FullProf software. The patterns along with the refinement data are plotted in Fig. 1. The XRD patterns confirm that the samples are pure in phase without any impurity peaks. Though the patterns are indexed to the T phase with P4 mm as the space group, the refinement reveals the coexistence of O phases in few compositions. Note that the % fraction of T phases is 88.5, 83.5, 94.7, and 97.9 and the % fraction of O phases is 11.5, 16.5, 5.3, and 2.1 for BST6, BST7, BST8, BST9, respectively. However, the compounds with a higher Sn concentration, BST10 and BST11, exhibit only the T phase. These changes in O and T phases with the composition can be seen from the presence of $(200)_O$, $(200)_T$, and $(002)_T$ peaks of the respective O and T phases shown in Fig. 1(b). The piezoceramics are known to undergo large structural transformation upon poling.[31–33] In order to understand the poling induced structural transformation in the present samples, the XRD patterns are recorded on all samples which are subjected to poling. Note that the poled pellets are ground into powder form 48 h after poling. The refinement analysis performed on the XRD patterns of poled samples (shown in

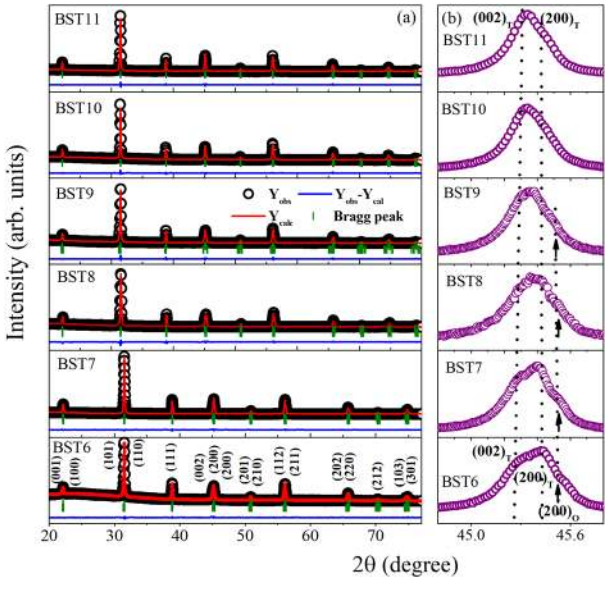

FIG. 1. The refined XRD patterns of BST6, BST7, BST8, BST9, BST10, and BST11 recorded at 300 K under un-poled conditions for the 2θ range from (a) 20 to 77° and (b) 44.8 to 45.8°.

Fig. S1, supplementary material) revealed a significant amount of increase in the O % phase fraction in comparison to the unpoled samples of BST6, BST7, BST8, and BST9. The XRD patterns of un-poled and poled samples in the 2θ range of 44.8°–45.8° and 65.4°–66.4°, corresponding to {200} and {220} planes, respectively, are shown in Fig. S2, supplementary material. The observed % phase fraction of the O phase is 26.5, 29.4, 23.4, 10.0, and 0.0 for BST6, BST7, BST8, BST9, and BST10, respectively, for the poled samples. Overall, with an increase in the Sn concentration, the system moves toward the T phase at 300 K in both un-poled and poled states.

The polarization (P) vs. electric field (E) measurement carried out on the samples revealed typical ferroelectric P–E hysteresis loops, and, as an example, the same is plotted in Fig. 2(a) for the BST7 sample. The extracted remnant polarization (P_r) is plotted as a function of composition in the inset of Fig. 2(a). The inset reveals that the maximum P_r (6.92 μC/cm^2) is observed for the BST8 sample, and it decreases with a further increase in the Sn concentration. To understand the dielectric behavior, the dielectric measurements are carried out at various frequencies. The temperature dependent real part of dielectric permittivity (ε') at 100 kHz is plotted in Fig. 2(b) for all samples. In order to show the shift in the transitions clearly, the ε' data are plotted on a relative scale. The samples exhibit a high dielectric constant, for example, the BST8 sample shows ~8000 as the dielectric constant maximum at 100 kHz. The detailed discussions on the dielectric characteristics of these samples are presented elsewhere.[25] Interestingly, the samples show anomalies in the dielectric spectrum at selected temperatures. These anomalies could be correlated with the structural phase transitions associated with the sample. The anomalies seen for the BST7 sample at 40 °C and 71 °C are associated with T to O phase transition ($T_{T\text{-}O}$) and paraelectric to ferroelectric phase transition (T_C), respectively.[34] As the Sn doping increases, T_C is shifted toward lower temperature and merges with $T_{T\text{-}O}$ for the compositions BST10 and BST11. As a consequence, the BST10 and BST11 samples show the T phase at 300 K without any O phase fraction, which is also evidenced from the XRD measurements.

To obtain the optical bandgap of the samples, the reflectance spectrum recorded on the samples, using UV-Visible diffused reflectance spectroscopy, is converted into the Kubelka–Munk function $F(R)$ using the equation: $F(R) = \frac{(1-R)^2}{2R}$, $R = 10^{-A}$. Here, R denotes the reflection coefficient of the material and A is the absorbance.[35] The Kubelka-Munk plot, which is a plot of $[F(R)h\nu]^2$ vs. the photon energy, is shown in Fig. 2(c) for BST7 (see Fig. S3, supplementary material for all other samples). The tangent of the plot, as shown in Fig. 2(c), making an intercept with the horizontal x-axis directly yields the bandgap of the respective sample. Since samples exhibit poling induced structural transformation, it is possible that they may show a change in their bandgap after poling. The Kubelka-Munk plots of the poled samples are shown in Fig. 2(c) and Fig. S4 of the supplementary material for BST7 and other samples, respectively. The obtained compositional variations of the bandgap before and after poling are plotted in Fig. 2(d). Note that the bandgap values show changes from 2.56, 2.61, 2.66, 2.78, 2.76, and 2.68 eV in the unpoled state to 2.86, 2.95, 2.96, 2.92, 2.97, and 2.95 eV after poling for BST6, BST7, BST8, BST9, BST10, and BST11 samples, respectively. It is to be noted that the bandgap variation with the composition does not follow a specific trend. However, the observed bandgap values advocate the suitability of the compounds for displaying PV characteristics under UV irradiation.

In order to probe the PV response of the BST samples, the current (I) vs. bias voltage (V) characteristics are measured under the dark and light illumination of 160 mW/cm^2, and the results are plotted in Fig. 3(a) for BST6, BST7, and BST8 and in Fig. 3(b) for BST9, BST10, and BST11 samples, respectively. Interestingly, all samples under study show typical ferroelectric PV characteristics with V_{OC} and short circuit current (I_{SC}). It is observed that V_{OC} progressively decreases with an increase in the doping concentration of BST7, i.e., 16 V, 11.3 V, 6.1 V, 4.5 V, and 4.5 V for BST7, BST8, BST9, BST10,

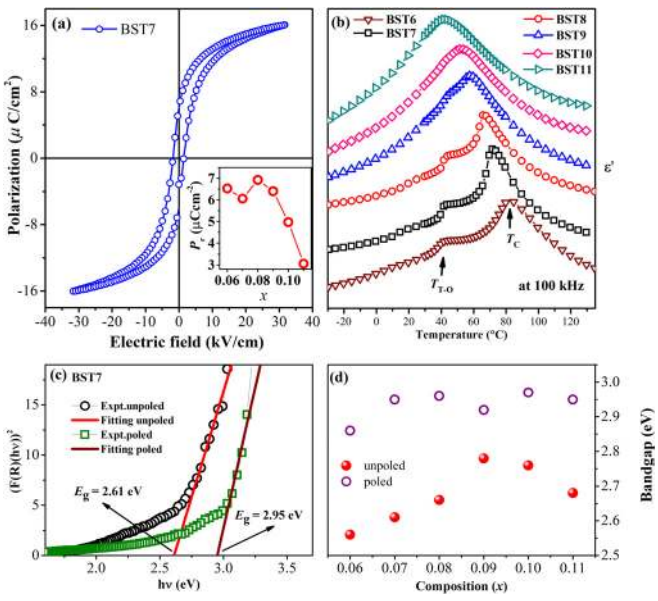

FIG. 2. (a) P vs. E curve for the BST7 sample. (b) Dielectric constant vs. temperature for BST6, BST7, BST8, BST9, BST10, and BST11 samples (the data are plotted on a relative scale). (c) $[F(R)(h\nu)]^2$ vs. $h\nu$ for unpoled and poled BST7 samples and (d) the bandgap plotted against the composition (x).

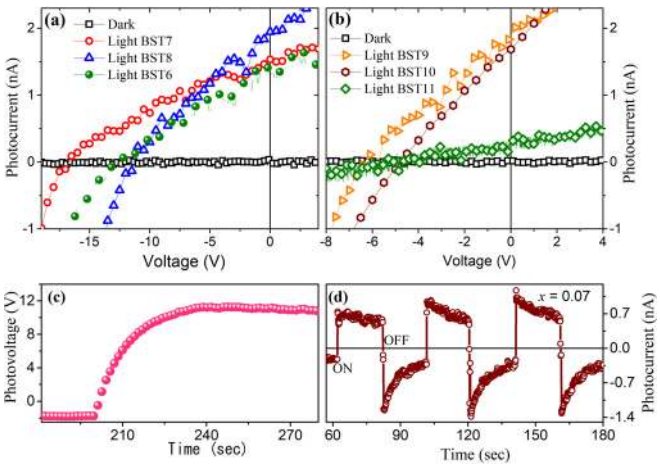

FIG. 3. I-V characteristics of (a) BST6, BST7, and BST8 and (b) BST9, BST10, and BST11 samples recorded under dark and light illumination. (c) V_{OC} vs. time and (d) photocurrent vs. time for the BST7 sample.

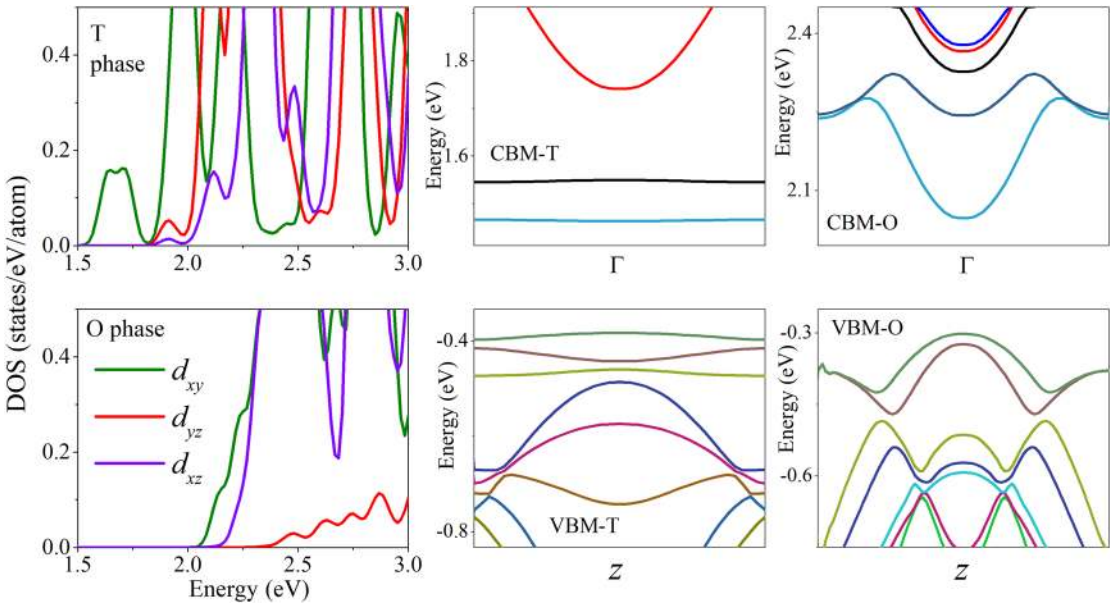

FIG. 4. Ti-d partial densities of states (PDOS) in the vicinity of CBM for the T and O phases of BST7. The band dispersion of T (middle panel) and O (right panel) phases of BST7 around band extrema and along the z-direction.

and BST11, respectively. Remarkably, the composition BST7 exhibits the maximum V_{OC} of 16 V. (Note that the PV study on the BST6 sample reveals the V_{OC} of 12.5 V, which is lower than that of the BST7 sample.) The stability of the photovoltage of BST7 is verified by measuring the photovoltage as a function of time under the zero-bias condition, and the respective plot is shown in Fig. 3(c). Similarly, the sharp current response to the light illumination is revealed in the plot shown in Fig. 3(d), where the measured current is plotted as a function of time under light ON and OFF states under the zero-bias condition. The value reported in this study is comparable to the recently reported giant PV effect in bulk $Ba_{1-x}(Bi_{0.5}Li_{0.5})_xTiO_3$.[1] Note that the compositional variation of V_{OC} in BST samples does not follow the variation in P_r where the maximum polarization is observed for the BST8 sample. Similarly, the change in V_{OC} as a function of Sn doping does not follow the variation in the bandgap either. Note that the bandgap shows nominal variation with Sn doping as seen from Fig. 2(d). This gives an indication that the polarization and the bandgap do not play a dominant role in the observed PV characteristics of the samples.

On the other hand, the observed compositional dependent PV response can be understood based on the structural symmetry of the compositions. Interestingly, Wang *et al.*[22] demonstrated the structural dependence of the bulk PV effect with respect to the shift current theory. Their calculations on different crystallographic phases of $KNbO_3$ suggest the dominance of rhombohedral and O phases in the PV response as compared to the T phase. In the present case, the samples BST6, BST7, BST8, and BST9 show the coexistence of T and O phases with 11.5, 16.5, 5.3, and 2.1 as % O phase fractions, respectively. Note that the phase fractions are estimated on samples in un-poled conditions. However, the PV measurements are carried out on samples poled at 2.5 kV/mm. Poling induced phase transitions are known in perovskite piezoceramics.[31–33] In particular, the $BaTiO_3$ based systems are reported to show the enhanced O phase at the expense of the T phase upon poling.[31–33] Hence, the BST samples subjected to PV measurements are expected to have higher O phase fractions than the estimated values. Keeping these factors in view, the observed large V_{OC} for BST7 and its variation with the Sn concentration could have strong structural correlation with the existing O phase. The decreasing trend in V_{OC} with an increase in the Sn concentration after BST7 could be the consequence of the decrease in O phase fractions along with an increase in the T phase. Note that V_{OC} remains constant (4.5 V) for $x = 0.10$ and 0.11, where only the T phase is seen.

In order to investigate the effect of symmetry breaking on the electronic structure and its consequent outcome on the PV response, the DFT calculations are carried out on the T and O phases of the BST7 compound. Figure 4 (left panel) shows the projected density of states (PDOS), which depicts the orbital composition around the region of the conduction band minimum (CBM) for T and O phases. It is seen from the figure that the antibonding Ti-d_{xy} states occupy the CBM, while the higher energy states are occupied by $d_{xz/yz}$ orbitals. Hence, there is a splitting of d_{xy} and $d_{xz/yz}$ orbitals. It is apparent that the O phase has mixing of the d_{xy} and $d_{xz/yz}$ orbitals, whereas in the T phase, the d_{xy} and $d_{xz/yz}$ states are well separated.

A larger hybridization among the d_{xy} and $d_{xz/yz}$ orbitals is observed in the O phase caused by a change in the crystal field, which leads to a mixing of these orbital characters in the CBM. In accordance with the shift current theory, if the CBM is more occupied by z-axis oriented orbitals (e.g., d_{xz}, d_{yz}, and d_{z^2-1}) and is extremely delocalized because of the stronger covalent interaction along the polarization direction (along the z-axis), this would yield a high shift current response, and as result, a substantial bulk PV is observed.[1,18,19,22] This suggests that the O phase shows an enhanced PV response, in comparison to the T phase. The results obtained from these DFT studies are in good agreement with our experimental observations.

Another significant factor that influences the PV response of the system is the mobility of the photo-generated charge carriers. The higher the mobility, the more the suppression of recombination of charge carriers, which in turn enhances the PV response. Since the effective mass varies inversely to the carrier mobility, materials with lower effective mass and hence higher mobility are suitable for the enhanced PV response.[36] Due to direction dependent dispersion in *k*-space, the effective masses are highly anisotropic. The effective mass along the z-direction (along the direction of current flow) is important for the superior PV response in ferroelectric systems like BTO. Figure 4 depicts the band dispersion of T (middle panel) and O (right panel) phases centering on the CBM and valence band maximum (VBM) along the *z*-direction in the reciprocal space. In the case of the T phase, the weakly dispersed band for both CBM and VBM of this phase will result in greater electron and hole effective masses, respectively, which will decrease the mobility of the photo-excited charge carriers along the *z*-direction. However, in the case of the O phase, the highly dispersed bands of CBM and VBM lead to lower electron and hole effective masses, thus considerably increasing the charge carrier mobility along the *z*-direction. This proves that the O phase exhibits an enhanced PV response compared to the T phase.

In conclusion, the $BaTi_{1-x}Sn_xO_3$ ($x = 0.06$, 0.07, 0.08, 0.09, 0.10, and 0.11) samples synthesized by the solid state method displayed a giant PV response, and the observed V_{OC} is found to decrease with an increase in the Sn concentration. The ferroelectric characterization revealed that the $x = 0.08$ sample showed the maximum P_r and hence is expected to demonstrate a large PV response. However, the $x = 0.07$ sample displayed the maximum V_{OC} (16 V) among other samples. This study illustrates that the change in V_{OC} with the composition did not follow the polarization and the bandgap variations but rather has strong correlation with structure symmetry. The XRD refinement elucidates that all samples exhibit the major T phase at 300 K. However, the coexisting O phase was seen in few compositions ($x = 0.06$, 0.07, 0.08, and 0.09). The variation in the % phase fraction of the O phase with the composition is in accordance with the variation in V_{OC}. The experimental findings are verified by the DFT calculations which prove that the O phase shows an enhanced PV response in comparison to the T phase. Overall, these studies correlate the observed PV response with the structural symmetry of the compound which is substantiated by the band-structure calculations.

See supplementary material for the refined XRD patterns of poled samples of all composition in the 2θ ranges of 20–70°, 44.8–45.8°, and 65.4–66.4°. The Kubelka–Munk plots of samples BST6, BST8, BST9, BST10, and BST11 showing the values of bandgaps.

We acknowledge Dr. Sudakar Chandran and Mr. Subhajit Nandy for allowing us to use the diffused reflectance spectroscopy equipment.

REFERENCES

[1] S. Pal, A. B. Swain, P. P. Biswas, D. Murali, A. Pal, B. R. K. Nanda, and P. Murugavel, Sci. Rep. **8**, 8005 (2018).
[2] Z. Xiao, Y. Yuan, Y. Shao, Q. Wang, Q. Dong, C. Bi, P. Sharma, A. Gruverman, and J. Huang, Nat. Mater. **14**, 193 (2015).
[3] F. Yang, M. Y. Han, and F. G. Chang, Sci. Rep. **5**, 11504 (2015).
[4] J. Huang, Y. Yuan, Y. Shao, and Y. Yan, Nat. Rev. Mater. **2**, 17042 (2017).
[5] C. Li and H. Wonneberger, Adv. Mater. **24**, 613 (2012).
[6] Y. Bai, G. Vats, J. Seidel, H. Jantunen, and J. Juuti, Adv. Mater. **30**, 1803821 (2018).
[7] V. M. Fridkin, IEEE Trans. Ultrason. Ferroelectr. Freq. Control **60**, 1551 (2013).
[8] J. E. Spanier, V. M. Fridkin, A. M. Rappe, A. R. Akbashev, A. Polemi, Y. Qi, Z. Gu, S. M. Young, C. J. Hawley, D. Imbrenda, G. Xiao, A. L. Bennett-Jackson, and C. L. Johnson, Nat. Photonics **10**, 611 (2016).
[9] C. Paillard, X. Bai, I. C. Infante, M. Guennou, G. Geneste, M. Alexe, J. Kreisel, and B. Dkhil, Adv. Mater. **28**, 5153 (2016).
[10] A. M. Glass, D. V. Linde, and T. J. Negran, Appl. Phys. Lett. **25**, 233 (1974).
[11] N. Ma and Y. Yang, Nano Energy **50**, 417 (2018).
[12] A. Bhatnagar, A. R. Chaudhuri, Y. H. Kim, D. Hesse, and M. Alexe, Nat. Commun. **4**, 2835 (2013).
[13] M. Qin, K. Yao, Y. C. Liang, and S. Shannigrahi, J. Appl. Phys. **101**, 014104 (2007).
[14] M. Qin, K. Yao, and Y. C. Liang, Appl. Phys. Lett. **95**, 022912 (2009).
[15] J. Zhang, X. Su, M. Shen, Z. Dai, L. Zhang, X. He, W. Cheng, M. Cao, and G. Zou, Sci. Rep. **3**, 2109 (2013).
[16] Y. Yuan, Z. Xiao, B. Yang, and J. Huang, J. Mater. Chem. A **2**, 6027 (2014).
[17] S. Y. Yang, J. Seidel, S. J. Byrnes, P. Shafer, C. H. Yang, M. D. Rossell, P. Yu, Y. H. Chu, J. F. Scott, and J. W. Ager, Nat. Nanotechnol. **5**, 143–147 (2010).
[18] S. M. Young and A. M. Rappe, Phys. Rev. Lett. **109**, 116601 (2012).
[19] L. Z. Tan, F. Zheng, S. M. Young, F. Wang, S. Liu, and A. M. Rappe, npj Comput. Mater. **2**, 16026 (2016).
[20] M. Nakamura, S. Horiuchi, F. Kagawa, N. Ogawa, T. Kurumaji, Y. Tokura, and M. Kawasaki, Nat. Commun. **8**, 281 (2017).
[21] A. Zenkevich, Y. Matveyev, K. Maksimova, R. Gaynutdinov, A. Tolstikhina, and V. Fridkin, Phys. Rev. B **90**, 161409 (2014).
[22] F. Wang and A. M. Rappe, Phys. Rev. B **91**, 165124 (2015).
[23] P. Poosanaas and K. Uchino, Mater. Chem. Phys. **61**, 36 (1999).
[24] Y. G. Yao, C. Zhou, D. C. Lv, D. Wang, H. J. Wu, Y. D. Yang, and X. B. Ren, Europhys. Lett. **98**, 27008 (2012).
[25] L. Kola, A. B. Swain, M. Rath, M. S. R. Rao, and P. Murugavel, Mater. Res. Bull. **106**, 371 (2018).
[26] G. Kresse and J. Furthmüller, Phys. Rev. B **54**, 11169 (1996).
[27] G. Kresse and D. Joubert, Phys. Rev. B **59**, 1758 (1999).
[28] J. P. Perdew, K. Burke, and M. Ernzerhof, Phys. Rev. Lett. **77**, 3865 (1996).
[29] J. D. Pack and H. J. Monkhorst, Phys. Rev. B **16**, 1748 (1977).
[30] D. Bagayoko, G. L. Zhao, J. D. Fan, and J. T. Wang, J. Phys.: Condens. Matter **10**, 5645 (1998).
[31] R. Garg, B. Narayana Rao, A. Senyshyn, P. S. R. Krishna, and R. Ranjan, Phys. Rev. B **88**, 014103 (2013).
[32] K. Brajesh, K. Tanwar, M. Abebe, and R. Ranjan, Phys. Rev. B **92**, 224112 (2015).
[33] A. K. Kalyani, H. Krishnan, A. Sen, A. Senyshyn, and R. Ranjan, Phys. Rev. B **91**, 024101 (2015).
[34] M. Deluca, L. Stoleriu, L. P. Curecheriu, N. Horchidan, A. C. Ianculescu, C. Galassi, and L. Mitoseriu, J. Appl. Phys. **111**, 084102 (2012).
[35] L. G. Devi, P. M. Nithya, and R. Kavitha, Mater. Today Commun. **17**, 391 (2018).
[36] J. Zhang, P. Zhou, J. Liu, and J. Yu, Phys. Chem. Chem. Phys. **16**, 20382 (2014).